Formation of Hydrogen Peroxide and Depletion of Oxalic Acid in Atmospheric Water by Photolysis of Iron(III)-Oxalate Complexes. Environ. Sci. Technol., 26, 1014-1022

ARTICLE *in* ENVIRONMENTAL SCIENCE AND TECHNOLOGY · NOVEMBER 1991

Impact Factor: 5.33 · DOI: 10.1021/es00029a022

Environ. Sci. Technol. 1992, 26, 1014–1022

Formation of Hydrogen Peroxide and Depletion of Oxalic Acid in Atmospheric Water by Photolysis of Iron(III)–Oxalato Complexes

Yuegang Zuo[†] and Jürg Holgné*

Swiss Federal Institute for Water Resources and Water Pollution Control (EAWAG), Swiss Federal Institute of Technology, ETHZ, CH-8600 Dübendorf, Switzerland

■ The generation of hydrogen peroxide (H_2O_2) and the depletion of oxalic acid by photochemical/chemical cycling of Fe(III)/Fe(II)–oxalato complexes in sunlight has been studied under the conditions typical for acidified atmospheric water. H_2O_2 is produced through the reduction of oxygen by intermediates formed from photoreactions of Fe(III)–oxalato complexes. The rate of H_2O_2 formation increases with sunlight intensity, and with oxalate and Fe(III) concentration within the concentration range used. This rate is 3.7 nM s^{-1} when 1 μM Fe(III) and 5 μM oxalate at pH 4 is exposed to September noon sunlight. Speciation calculations based on the concentration range of Fe(III) and oxalic acid in atmospheric water indicate that Fe(III)–oxalato complexes are often the predominant species of dissolved Fe(III). The concentrations of Fe(III)–oxalato complexes are sufficiently large to make their photolysis a dominant source of in-cloud H_2O_2, $O_2^{\bullet-}$, HO_2, and OH radicals and a major sink for atmospheric oxalic acid.

Introduction

The occurence of hydrogen peroxide (H_2O_2) in atmospheric water has significant consequences for atmospheric chemistry. Numerous expreiments have shown that H_2O_2 plays an important role in the acidification of cloud and rainwater through its participation in the oxidation of dissolved SO_2 to H_2SO_4 in the atmospheric liquid phase (*1–4*). This process is particularly important because H_2O_2 is highly soluble and the oxidation of SO_2 by H_2O_2 is relatively fast in acidic solution, whereas the oxidation of SO_2 by O_3 and the catalytic oxidation of SO_2 by O_2 in the presence of Fe and Mn is retarded at lower pH. The nonlinearity between the SO_2 emission and the wet deposition of sulfate suggests that a limiting factor in the acidification of precipitation is often the amount of H_2O_2 available to the cloud-precipitation system. In addition, H_2O_2 formation could be involved in radical chemistry, being a sink of HO_2 and a source of OH radicals (*5–10*); OH radicals are the most reactive oxidizing species for the transformation of atmospheric inorganic and organic pollutants.

It is now widely believed that the damage to forests by oxidants in North America and Central Europe may be more significant than the damage caused by acid rain deposition (*11*, *12*). This includes damage by H_2O_2 at concentrations typically measured in clouds, fogs, and rainwater.

All of these observations encourage much interest in the understanding of the mechanisms responsible for the formation and degradation of H_2O_2 in the atmospheric liquid phase. H_2O_2 has been extensively measured in the gas phase, in the atmospheric aqueous phase, and in cloud-, rain-, and fogwater as well as in snow and ice (*13–15*). The typical concentration range of H_2O_2 is 0.1–2 ppb in the gas phase and 10^{-7}–10^{-4} M in rain- and cloudwater, with the highest values generally observed in the summer.

The presence of H_2O_2 in the atmospheric liquid phase is usually assumed to arise solely from the dissolution of gas-phase H_2O_2 and the disproportionation of HO_2 radicals, which are produced by the photochemistry of atmospheric trace gases and scavenged by cloud droplets (*5*, *6*, *8*). However, Kleinman (*16*) has pointed out that the amount of H_2O_2 predicted by existing gas-phase photochemical models of the boundary layer (1 ppb) is insufficient in many instances to account for the in-cloud oxidation of SO_2 in summer rainwater. Zika et al. (*17*) did not observe any time dependence of the H_2O_2 concentration in rain during storms in South Florida and the Bahamas. They concluded that a substantial fraction of H_2O_2 in this case was generated within the cloudwater. It has also been reported that H_2O_2 can be produced in an aqueous solution through ozone decomposition, but these reactions are very slow in atmospheric water droplets (*18–21*). Kormann and co-workers (*22*) have suggested the photosensitized production of H_2O_2 by certain sunlight-absorbing semiconductor solids acting as sensitizers in cloudwater. The limited concentration data available for solid photosensitizers in precipitation suggest that this mechanism of H_2O_2 formation would require exceptional circumstances to be significant. It is clear that the sources of H_2O_2 in the atmospheric liquid phase are still far from being established.

Surprisingly, the in-cloud liquid-phase photochemical formation of H_2O_2 has received scant attention. Photochemical electron-transfer processes involving O_2, organic substances, and transition metals have been postulated to generate superoxide ions, $O_2^{\bullet-}$, in seawater (*23*). $O_2^{\bullet-}$ and its conjugate acid, the hydroperoxyl radical ($HO_2^{\bullet}$), undergo rapid disproportionation to yield H_2O_2 and O_2 in aqueous solutions such as atmospheric water (*10*). It is well-known that transition metals such as Fe, Mn, and Cu and organic ligands such as oxalic and pyruvic acid are common constituents of atmospheric water (*7*, *15*, *24–27*).

In this paper, we present the mechanistic and kinetic information for the photochemical formation of H_2O_2 and the decomposition of oxalic acid by sunlight-induced photolysis of Fe(III)–oxalato complexes, under experimental conditions which represent chemical conditions of acidified atmospheric water.

Background

Proposed Mechanism for the Photochemical Formation of H_2O_2 in Atmospheric Droplets. Most of the proposed mechanisms for the production of H_2O_2 in the aqueous phase involve the single-electron reduction of molecular oxygen to form the intermediate superoxide ion and its conjugated acid, the hydroperoxyl radical (denoted as $HO_2^{\bullet}/O_2^{\bullet-}$). The subsequent disproportionation of $HO_2^{\bullet}/O_2^{\bullet-}$ leads to H_2O_2 and O_2 formation:

$$HO_2^{\bullet}/O_2^{\bullet-} \xrightarrow{H^+} H_2O_2 + O_2 \qquad (1)$$

Transition metal ions such as Fe, Cu, and Mn can significantly influence this reaction, e.g., Fe(III) and Fe(II)

[†] Present address: Drinking Water Research Center, Florida International University, Miami, FL 33199.

 0013-936X/92/0926-1014$03.00/0

ions react with $HO_2^{\bullet}/O_2^{\bullet-}$ to form H_2O_2 and O_2, respectively:

$$HO_2^{\bullet}/O_2^{\bullet-} + Fe(II) \xrightarrow{H^+} H_2O_2 + Fe(III) \quad (2)$$

$$HO_2^{\bullet}/O_2^{\bullet-} + Fe(III) \xrightarrow{H^+} O_2 + Fe(II) \quad (3)$$

In the acidic pH range, however, the reaction with Fe(III) is very slow; the main fate of the HO_2 radical would be to react with Fe^{2+} to produce H_2O_2.

In addition to the scavenging from the gaseous phase, $HO_2^{\bullet}/O_2^{\bullet-}$ could be formed by several photochemical mechanisms in natural water. Light-absorbing organic substances can reduce oxygen either by direct electron transfer from the excited state of the organic compounds or by the generation of free electrons via photoionization. However, the production of free electrons is usually very slow in natural waters (*28–30*). It is also possible in natural waters that a photochemically induced electron transfer from complexing organic ligands (org) to oxidized metals (M^{n+}) occurs, and subsequently, the electron-deficient organic ligands further reduce O_2 to $O_2^{\bullet-}$. This pathway can be represented as

$$M^{n+}\text{–org} \xrightarrow{h\nu} M^{(n-1)+} + \text{org radical} \quad (4)$$

$$\text{org radical} + O_2 \rightarrow O_2^{\bullet-} + \text{oxidized org} \quad (5)$$

In the present study, Fe(III)–oxalato complexes were used as a model system to test this postulated mechanism for the photochemical formation of H_2O_2.

The photochemistry of Fe(III)–oxalato complexes has been widely studied, particularly in connection with UV and visible chemical actinometry (*31, 32*). The absorption of a photon by an Fe(III)–oxalato complex results in an electron transfer from a complexing oxalate ligand to the central ferric ion, producing a ferrous ion and an oxalate radical anion. The oxalate radical anion could reduce a further ferric–oxalato ion. In the presence of O_2, however, the oxalate radical anion would react with O_2 to produce $O_2^{\bullet-}$ in dilute solutions. Taking the monooxalato–ferric complex as an example, the mechanism could be expressed

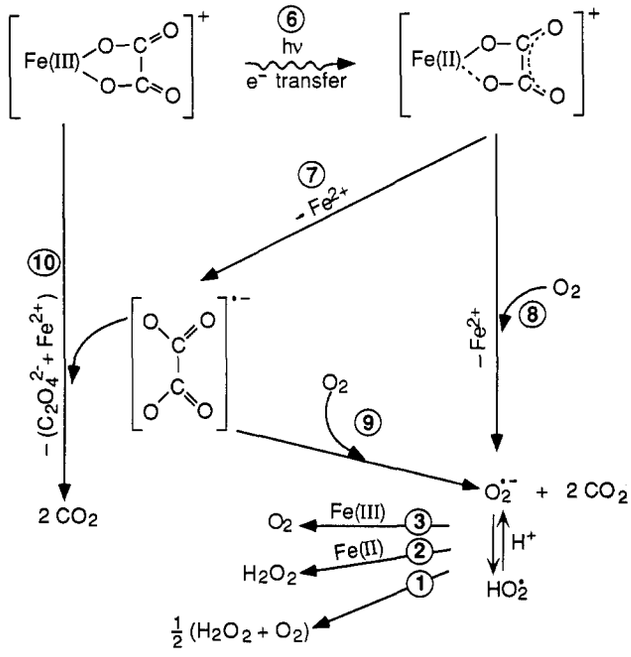

Figure 1. Scheme of possible photochemical reactions in the Fe(III)–oxalato–oxygen system.

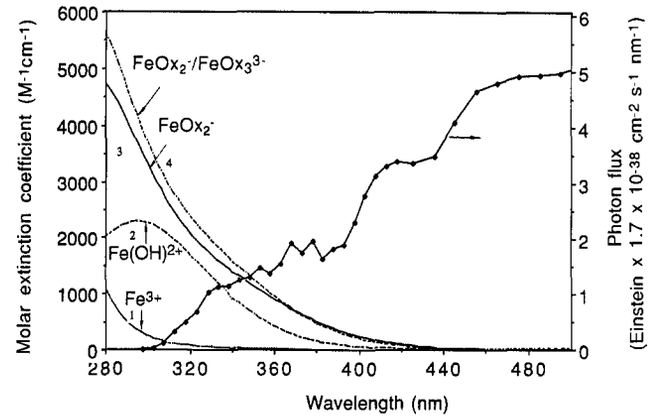

Figure 2. Absorption spectra of Fe(III)–oxalato complexes, $Fe(OH)^{2+}$ and Fe^{3+} in the region 290–500 nm. The absorption spectrum of $Fe(OH)^{2+}$ is obtained from Faust and Hoigné (*33*). Those for Fe(III)–oxalato complexes and Fe^{3+} were measured in this work using standard spectrophotometric techniques. The solar spectrum is obtained from Finlayson–Pitts and Pitts (*35*) and refers to a latitude of 47.4° N at noon on September 1st. The points indicate calculated averages over 5- or 10-nm intervals. 1, 10.0 μM $Fe(ClO_4)_3$ in 0.1 N $HClO_4$ (Fe^{3+} dominant), 2, 10.0 μM $Fe(ClO_4)_3$, pH 4 [$Fe(OH)^{2+}$ dominant], 3, 10.0 μM $Fe(ClO_4)_3$, 30 μM $K_2C_2O_4$, pH 4 (dioxalato dominant), 4, 10.0 μM $Fe(ClO_4)_3$, 120 μM $K_2C_2O_4$, pH 4 (tri- and dioxalato). All solutions contain 0.03 M $NaClO_4$ adjusted ionic strength.

by the scheme presented in Figure 1, which includes reactions 6–10. Analogous reactions can be written for the di- and trioxalato ions.

Occurrence, Speciation, and Photoreactivity of Fe(III)-Oxalato Complexes in Atmospheric Waters. The photochemistry of any aqueous Fe(III) complex depends on its speciation because different aqueous Fe(III) species exhibit different absorption spectra and photoreactivities. For instance, although the hexaaquo–Fe(III) complex photolyzes to produce OH radicals indirectly, its charge-transfer band does not significantly overlap the tropospheric solar spectrum. $Fe(OH)^{2+}$ and other hydroxide ion complexes have absorption bands that extend into the 290–400-nm region, overlapping the tropospheric solar specrum, and are therefore considered to be a major photochemical precursor to OH radical formation in the atmospheric liquid phase (*33, 34*). Fe(III)–oxalato complexes absorb even more strongly in the tropospheric solar UV–visible region (290–570 nm) (see Figure 2) and are also photochemically more reactive.

Dissolved iron is an ubiquitous constituent in atmospheric liquid water. Its concentration ranges from 10^{-7} to 10^{-4} M. In acidic atmospheric water, the hydroxide ion complexes $Fe(OH)^{2+}$ and $Fe_2(OH)_2^{4+}$ are the dominant species of Fe(III) in the absence of organic ligands (*33*). Extensive field measurements within the past several years have shown that chelate ligands are common in atmospheric water droplets (*15, 25–27*). Among these, oxalic acid is characteristic and important. This acid is mainly formed by the incomplete combustion, ozonolysis, and photooxidation of hydrocarbons in the gas phase or in atmospheric liquids. The decomposition of oxalic acid in the gas phase is very slow since it does not react with ozone, reacts very slowly with OH radicals, and is very slowly photolyzed under tropospheric conditions. On the other hand, since this acid is highly polar, it will be preferentially transferred into the liquid phase (at pH 4, apparent Henry's coefficient is 2.4×10^{11} M atm^{-1}). The concentration of oxalic acid in the atmospheric liquid phase can frequently reach a few tens of micromoles (*15, 25–27*). The presence of chelate ligands, such as oxalate, has a significant effect on the speciation and photoreactivity of Fe(III) ions in acidic

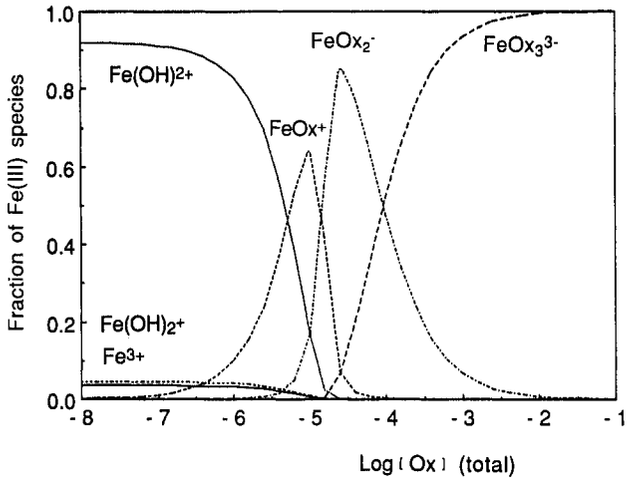

Figure 3. Mole-fraction distribution of the iron(III)–oxalate complexes based on the stability constants of the Fe(III)–oxalato species and Fe–hydroxo species (298 K, pH 4, [Fe(III)] = 10.0 μM, 0.03 M $NaClO_4$). Ox stands for oxalate.

atmospheric water since they may form stable complexes with Fe^{3+} ions:

$$Fe^{3+} + C_2O_4^{2-} \xrightarrow{K_{11}} Fe(C_2O_4)^+ \quad (11)$$

$$Fe(C_2O_4)^+ + C_2O_4^{2-} \xrightarrow{K_{12}} Fe(C_2O_4)_2^- \quad (12)$$

$$Fe(C_2O_4)_2^- + C_2O_4^{2-} \xrightarrow{K_{13}} Fe(C_2O_4)_3^{3-} \quad (13)$$

(For simplicity, water molecules in the coordinated sphere are not shown in the chemical formulas throughout this paper.) The speciation of dissolved Fe(III) in aqueous solution depends on the competition between the formation of Fe(III)–oxalato complexes and of Fe(III)–hydroxo complexes. Speciation calculations show that under the conditions of acidic atmospheric water droplets, where the pH ranges from 3 to 5, Fe(III)–oxalato complexes could be the predominant dissolved species (Figure 3). In contrast, Fe(II) mainly occurs as the hydrated cation.

Experimental Section

Materials. All chemicals were of reagent grade and were used without further purification. The water employed in all preparations was first deionized and then doubly distilled. The photolysis tubes were thoroughly cleaned with 1 M HCl solution and then finally with deionized–doubly distilled water. They were stored full of deionized–doubly distilled water. Before irradiation they were rinsed with the solution to be irradiated.

Irradiation Procedures. Solutions for irradiation were freshly prepared from air-saturated stock solutions of $Fe(ClO_4)_3$ in 0.1 M $HClO_4$ and potassium oxalate and adjusted to the desired pH with either $HClO_4$ or NaOH solutions. Except where noted, all solutions for irradiation contained 0.03 M $NaClO_4$ (to adjust the ionic strength), 10.0 μM Fe(III), and various concentrations of oxalate and were saturated with air. Deaeration, when desired, was accomplished by bubbling water-saturated high-purity N_2 through the solution for at least 15 min before irradiation.

Irradiations at 313 nm were carried out in cylindrical quartz photolysis tubes (1.5 cm i.d., containing 20 mL of solution) in a merry-go-round reactor (MGRR) equipped with a Hanau TQ 718 high-pressure Hg lamp (500 W) filtered through a Solidex borosilicate glass tube and a 2.0 mM K_2CrO_4 in 0.22 M K_2CO_3 aqueous filter solution with a minimum light path length of approximately 2.1 cm. The temperature was 20 ± 1 °C.

Irradiations in sunlight were performed using the same photolysis tubes held in a rack at a 30° angle from the horizontal and about 1 m above a black pavement. With this rack, the photolysis tubes could be put in and removed from sunlight within 1 s. All irradiations were centered on solar noon at EAWAG (Dübendorf, Zürich; 47.4° N 440-m elevation). The ambient temperature was 10–30 °C. The sunlight intensity (in mEinstein m^{-2} s^{-1}) was recorded every 10 min using a quantum sensor (Li-COR, LI-185) that responds to light of 400–700 nm. This measurement could give a value of 1.8 mEinstein m^{-2} s^{-1} at solar noon in June. Valerophenone was also used as a sunlight actinometer (responding to the UV B region)(*33*, *36*).

Analysis. H_2O_2 analysis was begun immediately after irradiation; all samples were analyzed within 40 min of irradiation. No significant concentration changes were detected during the analyses. The determinations were performed using a method based on the horseradish peroxidase- (POD-) catalyzed oxidation by H_2O_2 of *N*,*N*-diethyl-*p*-phenylenediamine (DPD) (*37*). The radical cation formed, $DPD^{\bullet+}$, is stabilized by resonance and forms a fairly stable absorption with a maximum at 551 nm and molar extinction coefficient (log base 10) ϵ = 21 000 ± 400 M^{-1} cm^{-1}. This method has been successfully applied to the analysis of hydrogen peroxide in freshwater, rainwater, and fogwater samples as well as during several laboratory research projects. For the case of clean water, the standard deviation for this method is 1%, and the lower limit of detection was 10 nM. The method is also somewhat sensitive to organic peroxides. The latter can be distinguished from H_2O_2 by examining the reaction kinetics of the radical cation $DPD^{\bullet+}$ formation, or by the use of catalase. Application of these techniques during our experiments indicated that no detectable organic peroxides were present in the irradiated samples. It is important to emphasize that all the concentrations of H_2O_2 measured are accumulated concentrations, that is, these do not include the H_2O_2 decomposed either during irradiation or by a subsequent rapid dark reaction with residual Fe^{2+}. The reason for this is explained in the Discussion.

Analysis of Fe(II) was carried out using the modified 1,10-phenanthroline colorimetric method of Tamura (*38*) and using a value of $\epsilon_{510} = 1.105 \times 10^4$ M^{-1} cm^{-1} for the Fe(II)–phenanthroline complex formed. Fe(III) stock solutions were standardized by reducing Fe(III) to Fe(II) with a solution of 1% ascorbate, in place of the NH_4F solution in Tamura's protocol, and measuring Fe(II).

Valerophenone (used for chemical actinometry) was analyzed by high-pressure liquid chromatography using a methanol–water mixture as the mobile phase and ODS-II as the stationary phase.

Measurement of the pH values was made with a Metrohm microcombination glass electrode with 3 M KCl as the inner reference solution, calibrated with Merck Titrisol pH 2, pH 4, and pH 7 standard buffers.

Oxalate was analyzed by DOC (dissolved organic carbon) determinations on a Dohrman DC-80 carbon analyzer. In some experiments, oxalate was measured by ion chromatography with conductivity detection. A Dionex Ionpac AG9 precolumn, a Dionex Ionpac AS9 column, and a Dionex anion micromembrane suppressor were used. Aqueous bicarbonate–carbonate solution was employed as eluent.

Electronic absorption spectra were obtained on a Uvikon Model 810 UV spectrophotometer.

Quantum Yields. Quantum yields, $\Phi_{\lambda Fe(II)}$, for the photochemical reduction of Fe(III) at wavelength λ = 313

Table I. Composition Matrix of the Iron(III)–Oxalate System in Perchloric Acid and the Equilibrium Constants

species	components Fe^{3+}	$C_2O_4^{2-}$	ClO_4^-	H^+	log β_t[a]	ref
Fe^{3+}	1	0	0	0	0	
$Fe(OH)^{2+}$	1	0	0	−1	−2.57	33
$Fe(OH)_2^+$	1	0	0	−2	−7.89	33
$Fe_2(OH)_2^{4+}$	2	0	0	−2	−3.22	33
$FeC_2O_4^+$	1	1	0	0	9.40	40
$Fe(C_2O_4)_2^-$	1	2	0	0	16.20	40
$Fe(C_2O_4)_3^{3-}$	1	3	0	0	20.78	40
$FeHC_2O_4^{2+}$	1	1	0	1	4.39	41
$FeClO_4^{2+}$	1	0	1	0	−0.32	42
$C_2O_4^{2-}$	0	1	0	0	0	
$HC_2O_4^-$	0	1	0	1	4.21	43
$H_2C_2O_4$	0	1	0	2	5.40	43
$HClO_4$	0	0	1	1	−1.58	44
ClO_4^-	0	0	1	0	0	
OH^-	0	0	0	−1	−14	
H^+	0	0	0	1	0	

[a] β_t is cumulative equilibrium constant.

nm were obtained by irradiating aqueous solutions of Fe(III)–oxalato complex under a N_2 atmosphere in the MGRR and measuring the initial rate of Fe(II) formation. Quantum yields were calculated according to the following equation

$$\Phi_{\lambda Fe(II)} = d[Fe(II)]/dt/2.303D\epsilon_\lambda[Fe(III)Ox_n]I_{\lambda 0}$$

where, $d[Fe(II)]/dt$ is the initial rate of Fe(II) formation at the wavelength λ, D is path length (cm), ϵ_λ is the decadic molar extinction coefficient of Fe(III)–oxalato complexes at wavelength λ (M^{-1} cm^{-1}), $[Fe(III)Ox_n]$ is the molar concentration of Fe(III)–oxalato complexes, and $I_{\lambda 0}$ is the volume-averaged incident light intensity at wavelength λ (einstein L^{-1} s^{-1}). $I_{313nm,0}$ was determined with the valerophenone actinometer, assuming a quantum yield of 1.0 (*36*).

Equilibrium Calculation. All speciation calculations in this paper were made with MICROQL, a chemical equilibrium program in BASIC developed by Westall (*39*). Values of the equilibrium constants were obtained from the literature and corrected using Davies equation for differences in ionic strength. The composition of the matrix for the complexes and the stability constants are collected in Table I.

Experimental Accuracy. The given points in the figures represent the data from single series of experiments. All experimental points are presented. The error within the series is not greater than 4% for H_2O_2 determination, 4% for Fe(II), and 5% for oxalate. Between series the errors are relatively larger due to variations of sunlight intensities. But under the experimental conditions employed, the experimental results between series are also well correlated to the irradiation intensities.

Results and Discussion

Stability of Oxalate. Oxalate was stable when exposed to 313-nm radiation under anoxic conditions. It was also stable for at least 1 h in oxygenated solutions at the concentration range used under 313-nm monochromatic light or under sunlight. In the dark, oxalate was not depleted even in the presence of Fe(III) under air-saturated conditions. The DOC of solutions was not decreased, and no hydrogen peroxide was formed under these conditions.

Oxygen Requirements for H_2O_2 Formation. A number of experiments were carried out in a nitrogen atmosphere, in which the initial concentration of Fe(III)

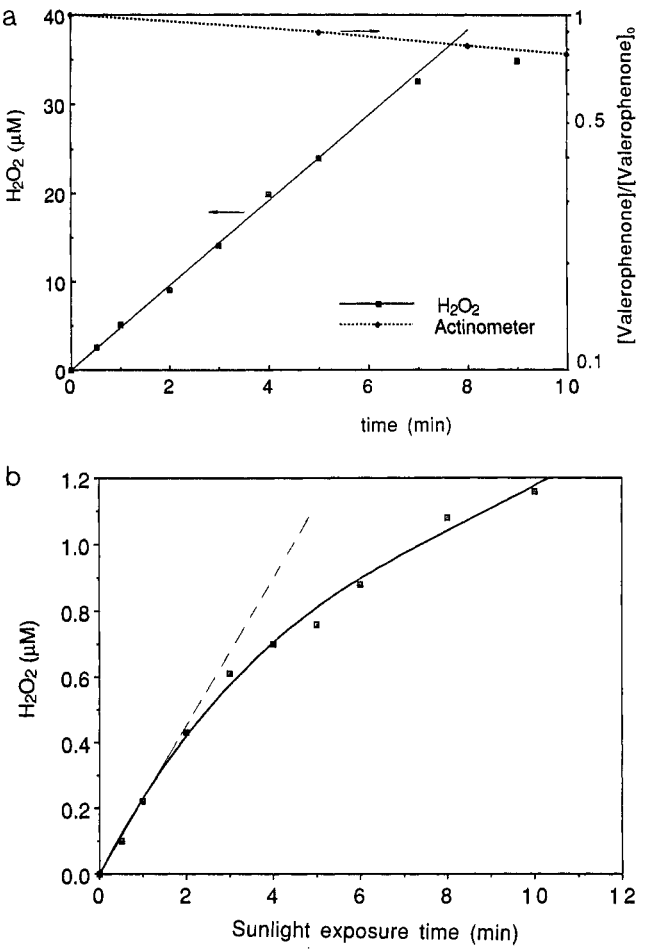

Figure 4. Hydrogen peroxide formation as a function of sunlight illumination time. Ionic strength, 0.03 M ($NaClO_4$, $HClO_4$); air saturated solution, at 283–300 K. (a) At solar noon on Sept 18, 1989 (I_0 = 0.63 mEinstein m^{-2} s^{-1}). $[Fe(III)]_0$ = 10 μM, pH = 3.96 ± 0.05, $[oxalate]_0$ = 120 μM. (b) On Sept 14, 1990 (I_0 = 0.62 mEinstein m^{-2} s^{-1}). $[Fe(III)]_0$ = 1.0 μM, pH = 3.92 ± 0.05, $[oxalate]_0$ = 5 μM. Valerophenone actinometer in deionized–tridistilled water (C_0 = 12 μM) was photolyzed simultaneously, in a separate photolysis tube.

was 10–100 μM, and that of oxalate 10–240 μM. Irradiations were carried out with 313-nm monochromatic light in the MGRR at temperatures of 20 and 30 °C, or in sunlight at ambient temperature. Under these conditions, no peroxide was formed. The amount of oxalic acid decomposed was equivalent to the amount of Fe(III) reduced in agreement with the following overall reaction:

$$2[Fe(C_2O_4)_n]^{(3-2n)+} \xrightarrow{h\nu} 2Fe^{2+} + (2n-1)C_2O_4^{2-} + 2CO_2 \quad (14)$$

The fact that hydrogen peroxide was only produced in oxygenated solutions indicates that oxygen is necessary for its formation. In air-saturated aqueous solutions, the oxygen concentrations is about 250 μM, much greater than that required for the formation of H_2O_2.

Photoformation of H_2O_2 in Sunlight. Figure 4a shows that the H_2O_2 formation was a linear function of the sunlight illumination time over wide concentration range of H_2O_2. The observed rate of formation of H_2O_2 in September noon sunlight was 80 nM s^{-1} in presence of 10 μM Fe(III) and 120 μM oxalate at pH 4 where trioxalato and dioxalato complexes are the predominant iron species (see Figure 3). Figure 4b shows the photoformation of H_2O_2 with a lower concentration of Fe(III) (1 μM) and oxalate (5 μM) at pH 4. In this case, the dominant iron species are dioxalate and monoxalate. They contribute 85% and

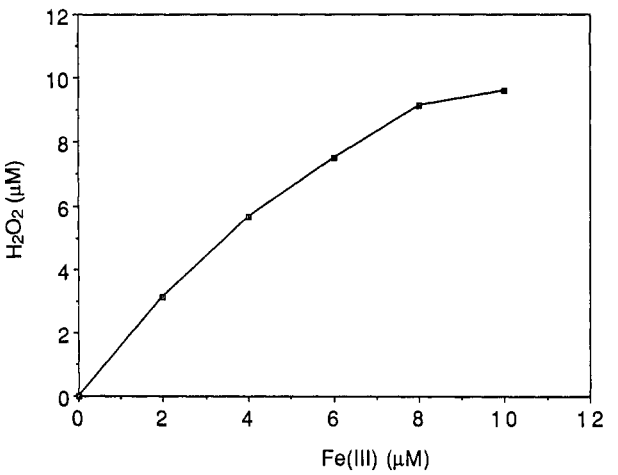

Figure 5. Hydrogen peroxide formation in sunlight as a function of Fe(III) concentration. Samples exposed for 3 min on Feb 7, 1990 (I_0 = 0.39 mEinstein m^{-2} s^{-1}). Solution composition is the same as for Figure 4a, except for Fe(III) concentration.

12% of total iron concentration, respectively. The initial rate of formation of H_2O_2 was 3.7 nM s^{-1}.

Concentraton Effects of Fe(III). To determine the dependence of H_2O_2 formation on the Fe(III) concentration, solutions at pH 4 containing 0–10 μM Fe(III), 120 μM oxalate, and 0.03 M $NaClO_4$ were irradiated. The formation of H_2O_2 in the solutions exposed to sunlight increased with increasing concentration of Fe(III) over the range 0–10 μM. In the absence of Fe(III), no H_2O_2 was detected (see Figure 5). The results are in accordance with speciation calculations which show that the total concentration of ferric–oxalato complexes increases linearly with Fe(III) under the above conditions.

Effects of Oxalate Concentration. To test the oxalate concentration effects, Fe(III) was held at 10 μM and the total oxalate varied from 0 to 240 μM. The results, presented in Figure 6, panels a and b, indicate that the accumulation of H_2O_2 in sunlight increased linearly with time and with oxalate concentration. The formation of H_2O_2 can be corrected for different light intensities. In the absence of oxalate, no H_2O_2 was observed. Cooper and DeGraff (*45*) have shown in their flash photolysis studies that excess oxalate retards the decay of the transient species produced in the primary photoreaction of Fe(III)–oxalato complexes. If the precursor of H_2O_2 formation, the superoxide ion $O_2^{\bullet-}$, is generated through the interaction of O_2 with the transient species, the formation rate of H_2O_2 would increase with oxalate concentration. This is in agreement with our experimental results and supports the mechanism proposed above.

pH Effects. Figure 7 demonstrates the effect of pH on the formation of H_2O_2. At the lower pH range 1.5–4.0, the H_2O_2 formation rate stayed at a rather high and constant value. Above pH 4.0, the rate of formation of H_2O_2 decreased with increasing pH. As discussed in the Background section, $HO_2^{\bullet}/O_2^{\bullet-}$ radicals undergo disproportionation to yield hydrogen peroxide and dioxygen by reactions 2 and 3. However, these reactions are strongly pH dependent. In the lower pH regime, $HO_2^{\bullet}$ (pK_a = 4.8) is the dominant species. Its reaction with Fe(II) to produce H_2O_2 is 2–3 orders of magnitude faster than with Fe(II) to form O_2. In the higher pH regime, however, $O_2^{\bullet-}$ becomes the dominant species. The reaction of $O_2^{\bullet-}$ with Fe(III), forming H_2O_2, is much slower than that with Fe(III), leading to O_2 [see Table II, in which we assume comparable concentrations of Fe(III) and Fe(II)]. Therefore, at the higher pH values the main product will

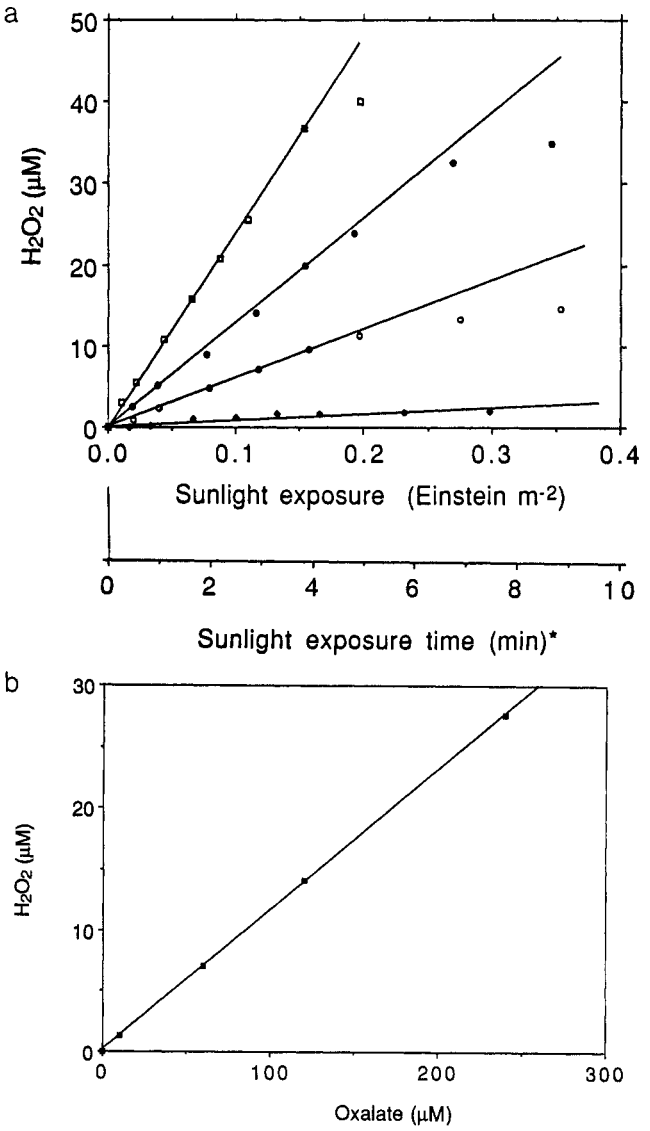

Figure 6. (a) Photoformation of hydrogen peroxide in sunlight with various oxalate concentrations. The solution composition is the same as for Figure 4a, except for oxalate concentration. Irradiations for oxalate concentration 60 and 120 μM were performed on Sept 18, 1989 (I_0 = 0.64 and 0.63 mEinstein m^{-2} s^{-1}, respectively), for oxalate concentration 10 and 240 μM on Sept 22, 1989 (I_0 = 0.55 and 0.36 mEinstein m^{-2} s^{-1}, respectively). (b) Hydrogen peroxide formation as a function of oxalate concentration (derived from Figure 6a, sunlight exposure = 113 mEinstein m^{-2}). (*) Time scale corresponds to I_0 = 0.63 mEinstein m^{-2} s^{-1}.

be O_2 rather than H_2O_2. In addition, above pH 5.5, the fraction of Fe(III)–oxalato complexes decreases sharply, which further reduces the possibility of H_2O_2 formation.

Oxalate Decomposition and Its Ratio to H_2O_2 Formation. Figure 8 shows the photodecomposition of oxalate in the presence of 10 μM Fe(III) and 120 or 240 μM oxalate at pH 4. Under these conditions, the photodegradation of oxalate had a half-life of a few minutes in September noon sunlight. Comparing the corresponding slopes in Figures 6a and 8 gives the quantitative relationship between the amount of H_2O_2 formed and the amount of oxalate consumed, $\Delta H_2O_2/\Delta$oxalate = 0.45 ± 0.05. This value decreases with increasing pH and with increasing iron concentrations. At lower pH and lower ion concentration, the ratio approaches the theoretical limit, 1 (data are not shown). Assuming a mechanism consisting of reactions 6–9, 2, and 3 in Figure 1 and Fenton reaction occurring simultaneously, the values of the mole ratio of hydrogen peroxide formed to oxalate consumed should lie

Table II. Reactions and Reaction Rate Constants for $HO_2^{\bullet}/O_2^{\bullet-}$ and H_2O_2 with O_3, Iron, and Copper Ions

	k, M^{-1} s^{-1}	ref	conc,[a] M	k',[b] s^{-1}
$HO_2^{\bullet}$ reactions				
$HO_2^{\bullet} + HO_2^{\bullet} \rightarrow H_2O_2 + O_2$ (1a)	8.3×10^5	46	10^{-8}	8.3×10^{-3}
$HO_2^{\bullet} + O_2^{\bullet-} \xrightarrow{H^+} H_2O_2 + O_2$ (1b)	9.7×10^7	46	10^{-9}	0.1
$HO_2^{\bullet} + Fe(III) \xrightarrow{-H^+} Fe(II) + O_2$ (3a)	$<10^4$	47	10^{-6}	$<10^{-2}$
$HO_2^{\bullet} + Fe(II) \xrightarrow{H^+} Fe(III) + H_2O_2$ (2a)	1.2×10^6	47	10^{-6}	1.2
$HO_2^{\bullet} + Cu(II) \xrightarrow{-H^+} Cu(I) + O_2$ (18a)	5×10^7	46	10^{-9}	5×10^{-2}
$HO_2^{\bullet} + Cu(I) \xrightarrow{H^+} Cu(II) + H_2O_2$ (19a)	1×10^9	46	10^{-9}	1
$O_2^{\bullet}$ reactions				
$O_2^{\bullet-} + HO_2^{\bullet} \xrightarrow{H^+} H_2O_2 + O_2$ (1b)	9.7×10^7	46	10^{-8}	1
$O_2^{\bullet-} + Fe(III) \rightarrow Fe(II) + O_2$ (3b)	1.5×10^8	47	10^{-6}	150
$O_2^{\bullet-} + Fe(II) \xrightarrow{H^+} Fe(III) + H_2O_2$ (2b)	1.0×10^7	47	10^{-6}	10
$O_2^{\bullet-} + Cu(II) \rightarrow Cu(I) + O_2$ (18b)	8×10^9	48	10^{-9}	8
$O_2^{\bullet-} + Cu(I) \xrightarrow{H^+} Cu(II) + H_2O_2$ (19b)	7×10^9	48	10^{-9}	7
$O_2^{\bullet-} + O_3 \xrightarrow{H^+} 2O_2 + OH^{\bullet}$ (20)	1.5×10^9	46	10^9	1.5
$H_2O_2^{\bullet}$ reactions				
$H_2O_2 + Fe(III) \rightarrow$ (17)	very slow	49		
$H_2O_2 + Fe(II) \rightarrow Fe(III) + OH^{\bullet} + OH^-$ (15)	76	49	10^{-6}	7.6×10^{-5}

[a] Assumed concentration values of the reactants for $HO_2^{\bullet}/O_2^{\bullet-}$ and H_2O_2 for noon summer scenario at pH 4; values are given only for exemplification of reaction rates and their competition. [b] Pseudo-first-order reaction rate constant based on k and the arbitrary concentration values of the reactants for $HO_2^{\bullet}/O_2^{\bullet-}$, H_2O_2, and O_3.

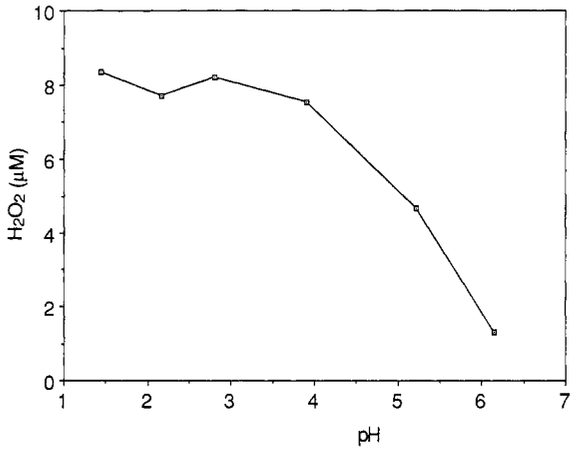

Figure 7. Effect of pH on the hydrogen peroxide formation. Samples exposed for 3 min on Feb 5, 1990 (afternoon I_0 = 0.22 mEinstein m^{-2} s^{-1}). The solution composition is the same as for Figure 4a, except for pH.

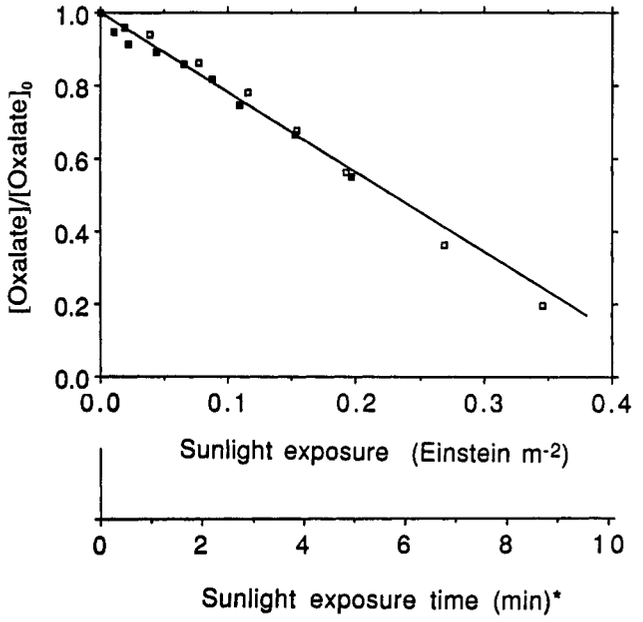

Figure 8. Decomposition of oxalic acid. The solution composition is the same as for Figure 4a, except for oxalate concentration. Irradiations of solutions containing 120 μM oxalate (open squares) and 240 μM oxalate (closed squares) were performed on Sept 18, 1989 (I_0 = 0.64 mEinstein m^{-2} s^{-1}) and on Sept 22, 1989 (I_0 = 0.36 mEinstein m^{-2} s^{-1}), respectively. (*) Time scale corresponds to I_0 = 0.63 mEinstein m^{-2} s^{-1}.

between 0 and 1. The qualitative agreement between these calculated values and the experimental results supports the proposed mechanism.

Stability of H_2O_2 in Solution. The results in Table III show that the H_2O_2 formed is quite stable after completion of irradiation. This is not surprising, although it is well-known that both Fe^{2+} and Fe^{3+} are capable of catalyzing the decomposition of hydrogen peroxide. The catalytic process involving Fe^{2+} can be described by the reactions 15 and 16:

$$Fe^{2+} + H_2O_2 \rightarrow Fe^{3+} + HO^{\bullet} + HO^- \quad (15)$$

$$Fe^{2+} + HO^{\bullet} \rightarrow Fe^{3+} + HO^- \quad (16)$$

In the presence of Fe^{3+} an additional reaction is involved according to the Haber–Weiss mechanism (*49*):

$$Fe^{3+} + H_2O_2 \rightarrow Fe^{2+} + HO_2^{\bullet} + H^+ \quad (17)$$

However, the ferric ion reacts much slower than ferrous ion with H_2O_2. In addition, catalysis by Fe^{3+} is sensitive to changes in the coordination environment of the ferric ion (*50*). The formation of the Fe^{3+}–oxalato complex in-

Table III. Stability of Photochemically Formed Hydrogen Peroxide

expt	irradiation time, min	Fe(III), 10^{-5} M	$K_2C_2O_4$, 10^{-6} M	H_2O_2 found at following times after completion of irradiation, μM: 10 min	1 h	1h/10 min, %
1	2	1	6	4.9	5.0	102
2	4	1	6	9.6	9.6	100
3	9	1	6	14.7	14.3	97
4	0.5	1	12	2.5	2.6	104
5	2	1	12	9.5	9.2	97
6	4	1	12	19.9	19.6	98
7	9	1	12	36.5	35.1	96

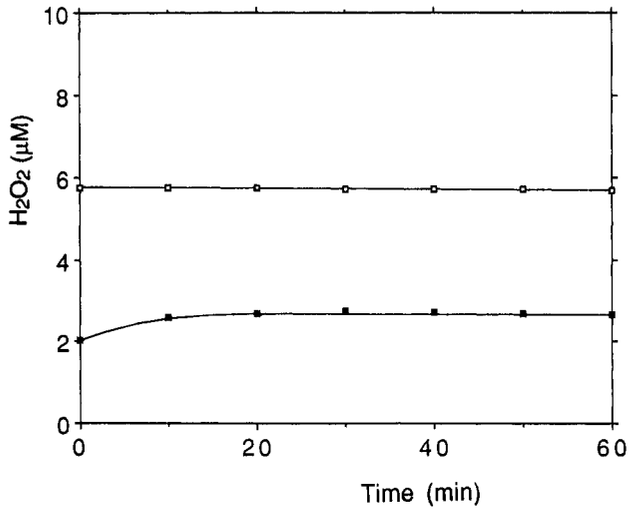

Figure 9. Inhibition of hydrogen peroxide decomposition and stabilization of hydrogen peroxide by oxalate (dark experiments). $[H_2O_2]_0$ = 5.8 μM, 0.03M $NaClO_4$, 30 μM oxalate at pH 4, air saturated (O_2 0.21 atm). Open squares, 10 μM Fe(III); closed squares, 10 μM Fe(II).

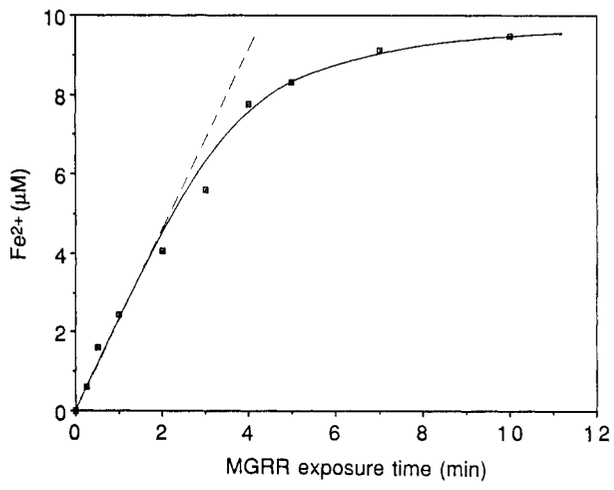

Figure 10. Photoproduction of Fe(II) from Fe(III)–oxalato complexes with monochromatic light (313 nm with bandwidth about 4 nm) in deaerated solutions. $[Fe(III)]_0$ = 10.0 μM, pH = 4.00 ± 0.05, $[oxalate]_0$ = 30 μM, ionic strength = 0.03 M ($NaClO_4$, $HClO_4$), deaerated using N_2 at 293 K, I_{313} nm = 0.60 μEinstein L^{-1} s^{-1} (valerophenone actinometer).

hibits the decomposition of H_2O_2 (*51*).

In the Fe^{2+}–H_2O_2–oxalate system, the decomposition of H_2O_2 was virtually instantaneous; before an initial sample could be taken, the hydrogen peroxide had been decomposed and Fe^{2+} simultaneously oxidized to Fe(III). (It should be noted that all values of the H_2O_2 concentration measured in this study are the values remaining after this reaction.) Subsequently, H_2O_2 was stabilized by the residual oxalate via complex formation. To confirm this point, the dark experiments were carried out with initial concentrations of 5.8 μM H_2O_2, 30 μM oxalate, and 10 μM Fe^{2+} or Fe^{3+} in the solutions saturated with air at pH 4. The results are shown in Figure 9.

Subsequent OH Radical Formation. Preliminary experiments were carried out with butyl chloride as a reference compound for OH radicals in the presence of an excess of octanol to control the lifetime of the OH radical (*52*). The results show that irradiating aqueous solutions containing Fe(III)–oxalato at pH 4 produces OH radicals. This production is due to the preceding formation of Fe(II) and H_2O_2. The addition of catalase inhibited the OH radical formation.

Photochemical/Chemical Cycle of Ferric and Ferrous Complexes. The overall stoichiometry for the photolysis of ferrioxalate in deaerated solution is expressed by eq 14. It indicates that for every ferrioxalate decomposed, there should be a corresponding gain of one Fe(II). Figure 10 depicts the photoproduction of Fe^{2+} with monochromatic light (313 nm) in the MGRR. The quantum yield determined from the initial slope is 1.2 ± 0.1, in good agreement with literature values (*32*). In the presence of O_2 (0.21 atm), we observed that 70% of the total iron was Fe(II) at steady state during irradiation. However, when the solution was placed in the dark for a few seconds after irradiation of a few minutes, only a small amount of Fe(II) remained. This observation could be significant, because of possible photochemical/chemical cycling between ferric and ferrous complexes if ferric–oxalato complexes, light, and O_2 are present. As illustrate in Figure 11, this cycling includes (i) the direct photolysis of Fe(III)–oxalato complexes; (ii) the reaction of the organic radical photoproducts with oxygen leading to $HO_2^{\bullet}/O_2^{\bullet-}$ radical formation, which leads to H_2O_2 production; and (iii) the subsequent reaction of these photooxidants with Fe^{2+}(aq), leading to the re-formation of Fe(III)– and Fe-

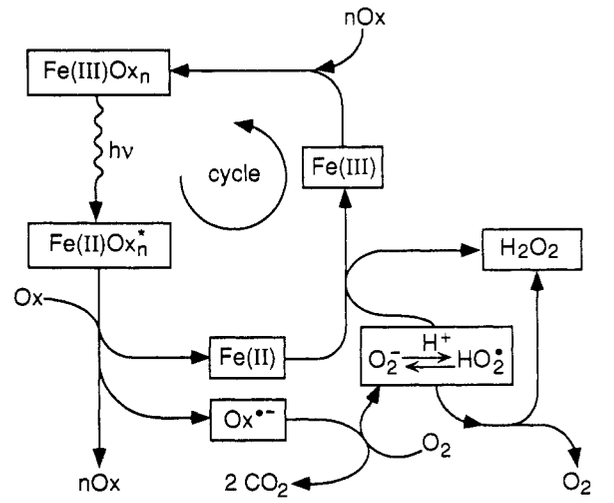

Figure 11. Scheme for the photochemical/chemical cycling of iron and the formation of H_2O_2.

(III)–oxalato complexes. The direct oxidation of photogenerated Fe^{2+}(aq) by O_2 has not been considered in Figure 11 because it is very slow at pH < 6. In the absence of complex ligand and light, the half-life for Fe(II) oxidation by O_2 at pH 4 is longer than 285 days (*53*). Although oxalate accelerates the oxidation of Fe(II), we did not observe any loss of Fe(II) after keeping the solution of 10 μM Fe(II) and 30 μM oxalate in 0.03 M $NaClO_4$ at pH 4 in the dark for 24 h. Even in the presence of 240 μM oxalate, only less than 2% of the Fe(II) was oxidized after 1 h in the dark. This indicates that the direct oxidation of Fe(II) by O_2 is insignificant under the conditions used.

The presence of oxalic acid, even at micromolar levels, considerably accelerates the photochemical/chemical cycling of iron. The complexation by oxalate not only increases the quantum yield for the photoreduction of Fe(III) from 0.14 (*33*) to 1.2 at 313 nm but also extends the absorption band into the visible region and increases the absorption coefficient (see Figure 2). Under conditions of similar sunlight intensities, the ferric oxalate in this study photolyzed about 2 orders of magnitude faster than the $Fe(OH)^{2+}$ previously studied (*33*). In September noon sunlight, the photoreduction of Fe(III)–oxalato complexes had a half-life of 17 s. Combining this half-life time with the steady-state ratio of Fe(III)/Fe(II), we estimate that

the photochemical/chemical cycling time for Fe(III)–Fe(II)–Fe(III) is of the order of minutes in a September clear day at noon. This cycling time is expected to decrease by a factor of 3 for a clear day at noon in June, even for in-cloud conditions owing to light-screening effects being compensated by light scattering.

Mechanism for Hydrogen Peroxide Formation. The above experimental results are consistent with the proposed mechanisms. H_2O_2 is produced via photochemical/chemical cycling of Fe(III)/Fe(II)–oxalato complexes as shown in the schematic diagram in Figure 11. It is not surprising, however, that in previous studies of the photolysis of the solutions of potassium ferrioxalate the formation of H_2O_2 in the presence of O_2 would not have been observed. These studies involved such high concentrations of oxalate that the oxygen, at relatively low concentrations in aqueous solution, was unable to compete for the photochemical intermediate. Thus, the oxalate radical formed in the primary photolysis would reduce another Fe(III)–oxalato complex rather than reduce oxygen (Figure 1):

$$Fe(C_2O_4)_n^{(3-2n)+} + C_2O_4^{\bullet-} \rightarrow Fe^{2+} + nC_2O_4^{2-} + 2CO_2 \quad (10)$$

In our system, the concentrations of Fe(III)–oxalato complexes ($\leq$10 μM) relative to oxygen (250 μM) are much lower, so reactions 8 and 9 (see Figure 1) have to be taken into account. Thus an oxygen molecule reacts either with an excited complex or with an oxalate radical to form $O_2^{\bullet-}$, which subsequently leads to H_2O_2 formation. The extent of H_2O_2 formation shows that reactions 8 and 9 compete efficiently with reaction 10.

That the amount of H_2O_2 formed can be many times greater than the initial concentration of Fe(III) in the presence of high oxalate concentrations (Figure 6a) is additional evidence for the occurrence of redox cycling between Fe(III) and Fe(II) (Figure 11). This cycling will continue until the oxalate is consumed.

Environmental Significance. Although direct dissolution of gaseous H_2O_2 and the disproportionation of HO_2 radicals scavenged by cloud droplets are currently considered to be the major sources of H_2O_2 in the atmospheric liquid phase, our results show that the photochemical generation of H_2O_2 from aqueous Fe(III)–oxalate complexes could be important. If, for example, 1 μM Fe(III) and 5 μM oxalate occur in an atmospheric droplet, their net contribution would be 3.7 nM s^{-1} of H_2O_2 at midday in autumn (Figure 4b). This value is similar to the calculated transfer rate of gas-phase H_2O_2 and the disproportionation of HO_2 free radicals taken up by small cloud droplets (ϕ = 12 μm) at midday in summer (*6*, *8*). In addition, preliminary experimental results show that both solutions of Fe(III)–pyruvate and Fe(III)–glyoxalate at pH 4.0 produce H_2O_2 in sunlight at a rate similar to Fe(III)–oxalate solutions. In many atmospheric water droplets, dissolved iron and oxalic, glyoxalic, and pyruvic acids are present in concentrations typically ranging from 0.1 to a few tens of micromoles (*15*, *25–27*). These facts indicate that the photolysis of Fe(III)–oxalato and other Fe(III)–organic complexes could be a major source of H_2O_2 in cloud, fog, and rainwater. It also should be noted that other transition metals, particularly Cu(II)/Cu(I), could also play a significant role in cloudwater H_2O_2 formation by catalyzing the disproportionation of $HO_2^{\bullet}/O_2^{\bullet-}$ involving a pathway analogous to that described for iron (*48*). For comparison, the relevant reactions and rate constants are presented in Table II. It should, however, be kept in mind that complex formation might greatly change the reactivity of transition metal ions. Further identification of organic and inorganic ligands for the transition metals in atmospheric water and studies of the interactions of the ligands with transition metals and the interaction of the complexes formed with sunlight are required.

Photolysis of Fe(III)–oxalato complexes produces Fe(II) ions. This has important implications for the production of OH radicals through the Fenton reaction as assumed in previous studies (*7*); during the nighttime, the Fenton reaction could be a major source of OH radicals in cloud droplets. Our preliminary experimental results have also shown that OH radicals are formed when high concentrations of Fe(III)–oxalate are illuminated. The formation rate is a few times higher than that in the absence of oxalate. Recently, Zepp et al. (*9*) have also quantified the formation of OH radicals by photo-Fenton reactions in aqueous solutions containing Fe(III)–oxalate complexes (100 μM) and H_2O_2. On the basis of the rate constants given in Table II, however, Fe(II) would be reoxidized mostly by $HO_2^{\bullet}/O_2^{\bullet-}$ under conditions of daytime irradiation. The production of OH radicals in atmospheric water droplets has considerable significance as they can oxidize a wide variety of natural and anthropogenic organic and inorganic substances. It would be interesting to investigate further the mechanism and kinetics of OH radical formation in the concentration ranges of dissolved iron and oxalate associated with atmospheric waters.

Removal of oxalic acid from atmosphere has received little attention to date. Grosjean (*54*, *55*) studied the photolysis of pyruvic acid in the atmospheric gas phase. He estimated that glyoxalic, pyruvic, and oxalic acids were photodegraded in a few hours. In the presence of cloud droplets, however, these acids will mostly transfer into liquid phase due to their large Henry's coefficient. Oxalic, glyoxalic, and pyruvic acids have been found at significant concentrations in rain, mist, fog-, and cloudwater (*15*, *25*, *26*, *56*, *57*). Based on the now presented results (Figure 8), the fast conversion of atmospheric oxalic and keto acids by photochemical/chemical redox cycling of iron can become a major sink for these compounds.

It should be noted that photochemical formation of H_2O_2 in liquid phase is nearly continuous and does not decline by the photodegradation of the dissolved oxalic and keto acids, because these acids are continuously resupplied by the "fresh" air and by in-cloud oxidation of other organic compounds.

This photochemical/chemical redox cycling of complexed iron species could also involve iron (hydr)oxide surfaces. Iron is photodissolved (*58*) and subsequently precipitated to the ocean and fresh surface water as a source of dissolved iron in these systems.

Conclusions

This study has shown that the formation of hydrogen peroxide by sunlight photolysis of Fe(III)–oxalato complexes could be a major source of H_2O_2 in the atmospheric liquid phase. Both dissolved iron and oxalic acid are ubiquitous pollutants in cloud-, fog-, and rainwater. The photolysis of Fe(III)–oxalate complexes produces oxalate radicals, and subsequently these radicals reduce oxygen to the superoxide ion leading to the formation of H_2O_2. About 1 H_2O_2 molecule is generated by every 2.2 molecules of oxalate consumed under conditions used. The formation rate of hydrogen peroxide is related to pH, sunlight intensity, and the concentrations of oxalate and dissolved iron. An increase in the concentration of oxalate and Fe(III) in the range of interest studied for atmospheric waters produces a corresponding increase in the H_2O_2 formation rate. Under conditions typical for cloudwater, H_2O_2 was produced at a significant rate and oxalate was simultaneously degraded with a half-life of a few minutes.

For instance, when a few micromolar oxalic acid and 1 μM dissolved iron are present, the accumulation rate of H_2O_2 is 3.7 nM s^{-1} in cloudwater in September noon sunlight. This rate is similar to or greater than that expected from the dissolution of gaseous H_2O_2 and disproportionation of HO_2 scavenged by cloud droplets under similar environmental conditions (*59*). The photolysis of Fe(III)–oxalato complexes could also be a major sink of atmospheric oxalic acid. In addition, it may have some implication for OH radical formation in cloudwater, particularly at nighttime, via the subsequent involvement of the Fenton reaction.

Acknowledgments

We are grateful to Werner Stumm for promoting these studies. We thank Janet G. Hering, Barbara Sulzberger, J. Alistair Kerr, and David Stocker for discussions and reviewing the manuscript. Our appreciation also goes to Heinz Bader for technical assistance and to H. Ambühl and R. Ribi for the light photometry data. We thank the reviewers for their recommendations.

Registry No. H_2O_2, 7722-84-1; oxalic acid, 144-62-7.

Literature Cited

(1) Calvert, J. G.; Lazrus, A.; Kok, G. L.; Heikes, B. G.; Walega, J. G.; Lind, J.; Cantrell, C. A. *Nature (London)* **1985**, *317*, 27–35.
(2) Chandler, A. S.; Choularton, T. W.; Dollard, G. J.; Eggleton, A. E. J.; Gay, M. J.; Hill, T. A.; Jones, B. M. R.; Tyler, B. J.; Bandy, B. J.; Penkett, S. A. *Nature (London)* **1988**, *336*, 562–565.
(3) Gervat, G. P.; Clark, P. A.; Marsh, A. R. W.; Teasdale, I.; Chandler, A. S.; Choularton, T. W.; Gay, M. J.; Hill, M. K.; Hill, T. A. *Nature (London)* **1988**, *333*, 241–243.
(4) Fung, C. S.; Misra, P. K.; Bloxam, R.; Wong, S. *Atmos. Environ.* **1991**, *24A*, 411–423.
(5) Schwartz, S. E. *J. Geophys. Res.* **1984**, *89*, 11589–11598.
(6) Chameides, W. L.; Davis, D. D. *J. Geophys. Res.* **1982**, *87*, 4863–4877.
(7) Graedel, T. E.; Mandich, M. L.; Weschler, C. J. *J. Geophys. Res.* **1986**, *91*, 5205–5221.
(8) McElroy, W. J. *Atmos. Environ.* **1986**, *20*, 427–438.
(9) Zepp, R.; Faust, B.; Hoigné, J. *Environ. Sci. Technol.* **1992**, *26*, 313–319.
(10) Weinstein-Lloyd, J.; Schwartz, S. E. *Environ. Sci. Technol.* **1991**, *25*, 791–800.
(11) Masuch, G.; Kettrup, A.; Mallant, R. K. A. M.; Slanina, J. *Int. J. Environ. Anal. Chem.* **1986**, *27*, 183–213.
(12) Möller, D. *Atmos. Environ.* **1989**, *23*, 1625–1627.
(13) Kelly, T. J.; Daum, P. H.; Schartz, S. E. *J. Geophys. Res.* **1985**, *90*, 7861–7871.
(14) Gunz, D. W.; Hoffmann, R. *Atmos. Environ.* **1990**, *24A*, 1601–1633.
(15) Zuo, Y. Photochemistry of Iron(III)/Iron(II) Complexes in Atmospheric Liquid Phases and Its Environmental Significance. Ph.D. Dissertation, ETH, Zürich, 1992.
(16) Kleinman, L. I. *Atmos. Environ.* **1984**, *18*, 1453–1458.
(17) Zika, R.; Saltzman, E.; Chameides, W. L.; Davis, D. D. *J. Geophys. Res.* **1982**, *87*, 5015–5017.
(18) Graedel, T. E.; Goldberg, K. I. *J. Geophys. Res.* **1983**, *88*, 10865–10882.
(19) Hoigné, J.; Bader, H. *Science* **1975**, *190*, 782–784.
(20) Zika, R. G.; Saltzman, E. S. *Geophys. Res. Lett.* **1982**, *9*, 231–234.
(21) Heikes, B. G.; Lazrus, A. L.; Kok, G. L.; Kunen, S. E.; Gandrud, B. W.; Gitlin, S. N.; Sperry, P. D. *J. Geophys. Res.* **1982**, *87*, 3045–3051.
(22) Kormann, C.; Bahnemann, D. W.; Hoffmann, M. R. *Environ. Sci. Technol.* **1988**, *22*, 798–806.
(23) Petasne, R. G.; Zika, R. G. *Nature (London)* **1987**, *325*, 516–518.
(24) Behra, Ph.; Sigg, L. *Nature (London)* **1990**, *344*, 419–421.
(25) Joos, F.; Baltensperger, U. *Atmos. Environ.* **1991**, *25A*, 217–230.
(26) Steinberg, S.; Kawamura, K.; Kaplan, I. R. *Int. J. Environ. Anal. Chem.* **1985**, *19*, 251–260.
(27) Norton, R. B.; Roberts, J. M.; Huebert, B. J. *Geophys. Res. Lett.* **1983**, *10*, 517–520.
(28) Draper, W. M.; Crosby, D. G. *J. Agric. Food Chem.* **1983**, *31*, 734–737.
(29) Sturzengger, V. Wasserstoffperoxid in Oberflaechengewaessern: Photochemische Produktion und Abbau. Ph.D. Dissertation, ETHZ, Zurich, 1989, No. 9004.
(30) Zepp, R.; Braun, A. M.; Hoigné, J.; Leenheer, J. A. *Environ. Sci. Technol.* **1987**, *21*, 485–490.
(31) Balzani, V.; Carassiti, V. *Photochemistry of Coordination Compounds*; Academic: New York, 1970; p 145.
(32) Hatchard, C. G.; Parker, A. C. *Proc. R. Soc. London, A* **1956**, *235*, 518–536.
(33) Faust, B. C.; Hoigné, J. *Atmos. Environ.* **1990**, *24A*, 79–89.
(34) Benkelberg, H. J.; Deister, U.; Warneck, P. OH quantum yield for the photodecomposition of Fe(III)–hydroxo compledes in aqueous solution and the reaction of OH with hydromethanesulfonate. In *Physico-chemical behaviour of atmospheric pollutants*; Restelli, G., Angeletti, G., Eds.; no. 23 in the Air Pollution Report Series of the Environmental Research Programme of the Commission of the European Communities, Directorate-General for Science, Research and Development; Kluwer Academic Publishers: Dortrecht, 1990; pp 263–269.
(35) Finlayson-Pitts, B. J.; Pitts, J. N., Jr. *Atmospheric Chemistry: fundamentals and experimental techniques*, 1st ed.; John Wiley & Sons: New York, 1986; p 1098.
(36) Zepp, R., U.S. Environmental Protection Agency, College Station Road, Athens, GA, personal communication, 1989.
(37) Bader, H.; Sturzenegger, V.; Hoigné, J. *Water. Res.* **1988**, *22*, 1109–1115.
(38) Tamura, H.; Goto, K.; Yotsnyanagi, T.; Nagayama, M. *Talanta* **1974**, *21*, 314–318.
(39) Westall, J. C. MICROQL, a chemical equilibrium program in Basic; Internal Report; EAWAG: CH-8600 Dübendorf, 1979.
(40) Lacroix, S. *Ann. Chim.* **1949**, *4*, 5–27.
(41) Bauer, R. F.; Smith, W. M. *Can. J. Chem.* **1965**, *43*, 2755–2762.
(42) Sutton, J. *Nature (London)* **1952**, *169*, 71–72.
(43) Schaap, W. B.; Laitinen, H. A.; Bailar, J. C., Jr. *J. Am. Chem. Soc.* **1954**, *76*, 5868–5872.
(44) Hood, G. C.; Reilly, C. A. *J. Chem. Phys.* **1960**, *32*, 127–130.
(45) Cooper, G. D.; de Graff, B. A. *J. Phys. Chem.* **1971**, *75*, 2897–2902.
(46) Bielski, B. H. J.; Cabelli, D.; Arudi, R.; Ross, A. *J. Phys. Chem. Ref. Data* **1985**, *14*, 1041.
(47) Rush, J. D.; Bielski, H. J. *J. Phys. Chem.* **1985**, *89*, 5062–5066.
(48) Von Piechowski, M. Der Einfluss von Kupferionen auf die Redoxchemie des Atmosphaerischen Wassers: Kinetische Untersuchungen. Ph.D. Dissertation, ETH, Zürich, 1991, No. 9512.
(49) Walling, C. *Acc. Chem. Res.* **1975**, *8*, 125–131.
(50) Jones, P.; Tobe, M. L.; Wyhne-Jones, W. F. K. *Trans Faraday Soc.* **1959**, *55*, 91–97.
(51) Weiss, J. *Faraday Soc.* **1947**, *2*, 188–196.
(52) Haag, W. R.; Hoigné, J. *Chemosphere* **1985**, *14*, 1659–1671.
(53) Stumm, W.; Morgan, J. J. *Aquatic Chemistry*; Wiley-Interscience: New York, 1981; p 780.
(54) Grosjean, D. *Atmos. Environ.* **1983**, *17*, 2379–2382.
(55) Grosjean, D. *Environ. Sci. Technol.* **1989**, *23*, 1506–1514.
(56) Kawamura, K.; Steinberg, S.; Kaplan, I. R. *J. Environ. Anal. Chem.* **1985**, *19*, 175–188.
(57) Baltensperger, U.; Kern, S. *J. Chromatogr.* **1988**, *439*, 121–127.
(58) Siffert, C.; Sulzberger, B. *Langmuir* **1991**, *7*, 1627–1634.
(59) Lelieveld, J.; Crutzen, P. J. *Nature* **1990**, *343*, 227–232.

Received for review August 9, 1991. Accepted January 2, 1992. This work was supported by the Presidential Foundation of the Swiss Federal Institute of Technology under the project title "Kinetics of Oxidation Processes in Cloud-, Fog-, and Rainwater: Role of Transition Metals".